Characterization of raw clay from N'Djamena (Chad) used in water treatment: the case of lead (Pb) in aqueous systems

Constant Allaramadji Ngarmadji , Youssouf Sawadogo, Joël Samba, Moustapha Sawadogo, Kassoum Barry, Mohamed Seynou, Lamine Zerbo

Journal de la Société Ouest-Africaine de Chimie
J. Soc. Ouest-Afr. Chim. (2026), 055 : 30 - 44
31ème Année, 2026

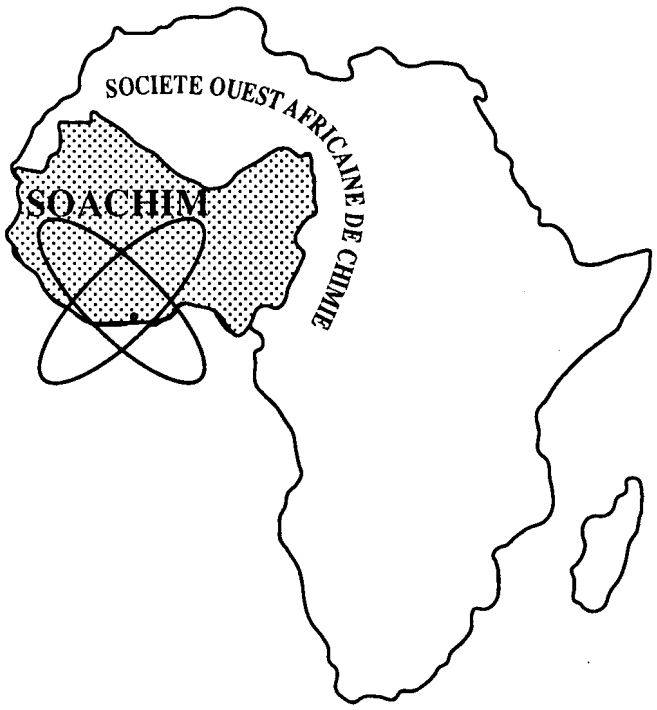

ISSN 0796-6687
Code Chemical Abstracts : JSOCF2
Cote INIST (CNRS France) : <27680>
Site Web: http://www.soachim.info

Characterization of raw clay from N'Djamena (Chad) used in water treatment: the case of lead (Pb) in aqueous systems

Constant Allaramadji Ngarmadji [1,2], Youssouf Sawadogo[1,3*], Joël Samba[1], Moustapha Sawadogo[1], Kassoum Barry[1,4], Mohamed Seynou[1], Lamine Zerbo[1*]

[1]Molecular and Materials Chemistry Laboratory (LC2M), University Joseph KI-ZERBO, B.P. 7021 Ouagadougou 03, Burkina Faso

[2]University of N'Djamena, Faculty of Exact and Applied Sciences, B.P. 1117, N'Djamena, Tchad

[3]Tenkodogo University Center, Thomas SANKARA University, 12 B.P. 417 Ouagadougou 12, Burkina Faso

[4]Lédéa Bernard OUEDRAOGO University, 01 BP 346 Ouahigouya 01, Burkina Faso

(Reçu le 25/03/2026– Accepté après corrections le 30/08/2026)

Abstract: This study evaluates the potential of a natural clay from N'Djamena (Chad) for removing Pb^{2+} ions from aqueous solutions under static conditions. The adsorption performance was interpreted using Langmuir and Freundlich isotherm models. Mineralogical characterization classified the raw material as a clay soil, predominantly composed of kaolinite (49.3%), with contributions from goethite (15.8%), quartz (18.1%), vermiculite (1.5%), and k-feldspar* (15.4%). The clay is primarily composed of silica (40.46%), alumina (23.84 %), and iron oxide (14.44%). Its specific surface area is 86.82 m^2/g. It has a cation exchange capacity of 46 meq/100 g and a swelling index of 2.71 cm^3/g. Optimal lead removal was achieved under the following conditions: 25 mL of solution per reactor; a clay-solute contact time of 90 minutes; an initial Pb^{2+} concentration of 20 µg/L; and a pH of 7. The adsorption of lead onto the studied clay is well described by the Langmuir isotherm, with a maximum adsorption capacity of 14.64 µg/g. Kinetic analysis suggests that the pseudo-second-order model accurately represents the adsorption process. These results show that the clay is an effective natural material for removing lead from water, suggesting its potential use in water treatment.

Keywords: clay; characterization; Pb^{2+} ions; water treatment

Caractérisation d'une argile de N'Djamena (Tchad) utilisée dans le traitement de l'eau : le cas du plomb (Pb) dans les systèmes aqueux

Résumé : Cette étude évalue le potentiel d'une argile naturelle de N'Djamena (Tchad) pour l'élimination des ions Pb^{2+} en solution aqueuse. Les performances d'adsorption ont été étudiées et interprétées à l'aide des modèles de Langmuir et de Freundlich. La composition minéralogique est dominée par la kaolinite (49,3 %), le quartz (18,1 %), la goethite (15,8 %), de feldspath (15,4 %) et de vermiculite (1,5 %). La silice (40,46 %), l'alumine (23,84 %) et l'oxyde de fer (14,44 %) dominent la composition chimique. La surface spécifique déterminée est 86,82 m^2/g, tandis que sa capacité d'échange cationique est évaluée à 46 meq/100 g et son indice de gonflement à 2,71 cm^3/g. Le protocole expérimental a consisté à utiliser 25 mL de solution par réacteur, avec une concentration initiale en Pb^{2+} de 20 µg/L, un pH de 7 et un temps de contact de 90 min. Dans les conditions optimales, l'adsorption du plomb suit l'isotherme de Langmuir (Q_{max} = 14,64 µg/g) et une cinétique de pseudo-second ordre. Ces résultats confirment l'efficacité de l'argile étudiée pour la rétention du plomb et son potentiel pour le traitement des eaux.

Mots Clés : argile ; Pb^{2+} ; caractérisation ; traitement d'eau

[*] **Auteurs de correspondance** : Youssouf SAWADOGO, E-mail address: s.youssouf@ymail.com

Lamine ZERBO, E-mail address: lamine_zerbo@yahoo.fr

1. Introduction

Clay is one of the most essential components of the Earth's crust and plays a pivotal role in biotopes [1]. These minerals exhibit highly distinctive properties and occur in nearly inexhaustible quantities in certain countries, including Chad. Despite the considerable quantity of clay available in N'Djamena, its utilization is predominantly confined to the domains of housing and traditional ceramics [2]. The scientific literature pertaining to Chad's clays is scant, with a paucity of studies addressing their physicochemical, chemical and mineralogical characteristics [3-5]. The extant research on the application of Chadian clays in pollution control is notably limited. In major urban areas of Chad, the public drinking water supply remains inadequate, resulting in populations relying on untreated groundwater and surface water sources. It is particularly evident that communities situated along the Chari and Logone rivers in the capital city directly utilize river water without the necessity of prior treatment. It has been reported by several studies that these waters are contaminated by microbial, inorganic and organic pollutants, which pose a significant risk to human health [6, 7]. Consequently, these water resources require appropriate treatment prior to human consumption.

In the domain of water pollution control, clays have been extensively utilized due to their substantial adsorption capacity and ubiquitous availability. A substantial body of research has been dedicated to the removal of pollutants from aqueous systems and the associated pollution indicators [8-10]. An extensive programme of research has been conducted on the capacity of natural and modified clays to adsorb heavy metals, with a particular focus on lead (Pb^{2+}).

Lead (Pb) is a toxic trace metal that can contaminate surface water from various natural or anthropogenic sources. Its presence in water can lead to deterioration in water quality when its concentration exceeds the permissible thresholds defined by WHO and EU standard (≤ 10 µg/L) [11, 12]. The US Environmental Protection Agency (USEPA) has a guideline value of 15 µg/L in drinking water [13]**.** It is therefore essential to minimize lead exposure through systematic monitoring of water quality. In instances of contamination, the implementation of appropriate treatment processes is imperative for the removal of pollutants and the mitigation of their impact.

The objective of this study is to evaluate the capacity of N'Djamena clay to remove lead from aqueous solutions through a detailed characterization of its physicochemical, chemical, and mineralogical attributes. The present study investigates the impact of solution pH, clay mass, contact time, and initial lead concentration on adsorption performance, with the objective of determining the conditions that optimize lead removal.

2. Materials and method

2.1. Materials

The geographical area under consideration is located in central-western Chad, at the confluence of the Chari and Logone rivers, on the right bank of the Chari. The region is predominantly composed of floodplains that were formed during the late Quaternary period. The presence of low-lying depressions is a pervasive phenomenon, with some of these depressions exhibiting the capacity to temporarily retain rainwater following the rainy season [14]. Geolocation of the sampling site was performed with a GARMIN 12XL GPS (12°03′15.1″N, 15°06′58.5″E), and the sampling areas are depicted in **Figure 1**. The clay in question is denoted TKA and is extracted from the clay site of Toukra. The selection criteria included clay abundance, soil type, and site accessibility, with an estimated clay reserve of 2.48×10^6 m³.

The prospecting and sampling procedures were conducted in accordance with the methodology described by Pansu et al. (1997) [15]. The drilling of wells was conducted to depths ranging from 1.5 to 3.0 metres, with the precise depth determined by the specific characteristics of each site. Sampling was carried out in situ using a hand auger, a method that involves the use of a manual pump to extract samples from the well. A representative quantity for laboratory analysis was obtained using the quartering method. The clay sample was subjected to a process of crushing and sieving, with the resultant material passing through a 80 µm sieve. The analytical sample was then prepared in accordance with the procedure delineated in **Figure 2**.

In the environment, lead is found to occur in two oxidation states. +2 and +4. The tetravalent state, despite its high degree of oxidizing ability, is seldom observed in nature. In contrast, the divalent state is the most stable and prevalent [16]**.** Depending on the objectives of the experiment, a number of working solutions were subsequently obtained by dilution.

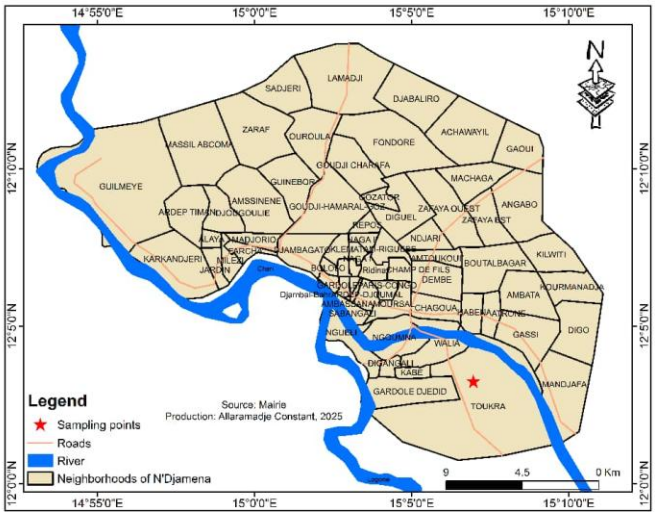

Figure 1: Location of TKA sampling Site

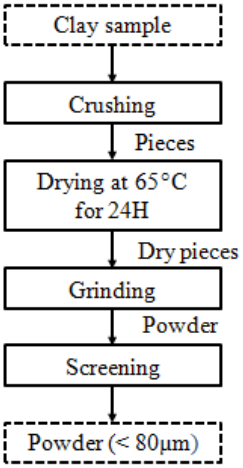

Figure 2: Diagram of analytical preparation

2.2. Experimental methods

These analyses were conducted to investigate the physicochemical properties directly affecting the adsorption capacity of the clay TKA, as well as its chemical and mineralogical characteristics.

The determination of texture was conducted in accordance with the Robinson pipette method, as stipulated in the AFNOR NF X31-107 standard [17]. Textural classification was based on the USDA/FAO (1938) texture triangle [18]. This involves placing the proportions of sand, silt and clay in a triangle. The intersection of these three proportions provides the texture of the TKA sample.

The moisture content was determined by measuring the loss of mass of the sample at a constant temperature of 105°C. The mass loss was then calculated using equation (1) [19].

$$\%\boldsymbol{H} = \frac{\boldsymbol{m_1 - m_2}}{\boldsymbol{m_1}} \times \mathbf{100} \qquad \textbf{(1)}$$

Where H is moisture content, m_1 (g) is mass of wet sample and m_2 (g) is mass of sample dried at 105 °C. For the moisture content analysis, the sample was subjected to oven heating, with a temperature ramp of 5°C/min to 1000°C applied, after which the sample was held for a duration of one hour. Subsequently, the sample was subjected to a cooling process in a drawer for a period of four hours prior to undergoing a weighing procedure [19]. The loss on ignition (LOI) was determined using the following equation (2).

$$\boldsymbol{LOI} = \frac{\boldsymbol{m_2 - m_3}}{\boldsymbol{m_2}} \times \mathbf{100} \qquad \textbf{(2)}$$

Where $\mathbf{m_2}$ (g) represents the mass of the sample dried at 105 °C, and $\mathbf{m_3}$ (g) denotes the mass of the sample after ignition.

ASTM D854-23 standard was used to determine the relative density of the clay material [20].

The pH and electrical conductivity of the clay material were determined using a pH meter (CG822) and a conductivity meter (HQ40d). The pH was measured accordance with international standard ISO 10390 [21] and conductivity according to ISO 11265:2025 [22].

The pH at the point of zero charge (pH_{pzc}) was determined using the method described by Tchakala *et al*. (2012) [23]. The procedure involved mixing clay with sodium nitrate solution. The initial pH ($\mathbf{pH_i}$) was adjusted between 2 and 8 using 0.1 M HCl or NaOH. The suspension was stirred for 24 h, after which the final pH ($\mathbf{pH_f}$) was recorded. The point of zero charge (PZC) was determined from the intersection of the $\mathbf{pH_f = f(pH_i)}$ curve with the first bisector.

Swelling index (SI) was determined by placing 2 g of clay in 10 mL of water within a graduated test tube. The swelling index, expressed in cm³ per 2 g of TKA , corresponds to the volume occupied by the sample [24].

In order to ascertain the colloidality of the substance under investigation, 4 mg of TKA were suspended in 100 mL of water, and 0.2 mg of magnesium oxide were then added with the objective of inducing deflocculation. The mixture was stirred for 5 minutes and transferred to a graduated test tube. Following a 24-hour period, the volume of the resultant liquid was measured, and the colloidality was calculated using the following formula (3) [25]:

$$\boldsymbol{C} = \mathbf{100} - \boldsymbol{V} \qquad \textbf{(3)}$$

Where $\boldsymbol{C}$ (%) represents colloidality, and $\mathbf{V(mL)}$ denotes the volume of the supernatant.

The cation exchange capacity (CEC) and exchangeable bases were determined using the

ammonium acetate method, in accordance with the AFNOR NF X31-130 standard [26].

The sample was analyzed by nitrogen adsorption at 77 K using a Nova 800 BET analyzer. Specific surface area was calculated from the adsorption data in accordance with ASTM C1069-09 [27].

The organic matter (OM) content was determined using the Walkley-Black method, as described by Pauwels et al. (1992) [28]. The organic carbon was oxidized with 1 N $K_2Cr_2O_7$ in H_2SO_4, and the excess dichromate was titrated with ferrous sulphate. The OM content was calculated using Van Bemmelen's conversion factor [28].

The TKA sample (< 80 µm) was further ground, and then 10.0 g was homogenized with 0.8 g of four additives using an RS200 vibrating disc mill for 3 minutes. The resulting powder was compressed into pellets and analyzed by X-ray fluorescence (S8 TIGER) to determine the composition of the main oxides.

To identify the various mineral phases, powder diffraction method was employed, which involves analysis of a completely disoriented powder. Analysis was conducted using a Phillips PW1710 diffractometer operated at 40 kV and 40 mA, over a 2θ range of 5° to 70°. The diffractogram was analyzed using Origin 6.0 software, and the mineral phases were identified by comparison with Powder Diffraction File (PDF) and the open-access Crystallography Open Database (COD).

Mineralogical analysis was conducted based on the chemical composition determined by X-ray fluorescence. Mineralogical calculations were performed using the relationship proposed by Yvon et al. (1982) in equation (4) [29].

$$\boldsymbol{T_a = \sum_{i=1}^{n} M_i \times P_i(a)} \quad \textbf{(4)}$$

Where $\mathbf{T_a}$ (wt.%) denotes the clay content, $\mathbf{M_i}$ (wt.%) represents the content of mineral **i** in the clay, and $\mathbf{P_i(a)}$ (wt.%) corresponds to the proportion of the oxide in mineral **i**.

Fourier Transform Infrared (FTIR) spectrum of TKA was recorded using a Vertex 70 DTGS spectrometer. Sample mixture was pressed into a pellet prior to analysis. Spectra were acquired over the range 4000 - 400 cm^{-1} with a spectral resolution of 4 cm^{-1}. The resulting transmittance spectrum as a function of wavenumber was interpreted to identify the functional groups present on the clay surface.

Retention tests were performed under static conditions by contacting the synthetic solution with the clay material. The mixture was stirred at room temperature, and pH of the solution was adjusted using 0.1 N sulfuric acid (H_2SO_4) or 0.1 N sodium hydroxide (NaOH).

At the end of each experiment, the mixture was filtered sequentially using Whatman No. 4 paper followed by a 0.45 µm membrane syringe filter. Residual lead concentrations in the filtrates were measured using a HACH DR3900.

Adsorption capacity ($\mathbf{Q_{ads}}$) and lead removal efficiency (**R**) were calculated using equation (5) and (6).

$$\boldsymbol{Q_{ads} = \frac{C_0 - C_r}{m} \times V} \quad \textbf{(5)}$$

$$\boldsymbol{R = \frac{C_0 - C_r}{C_0} \times 100} \quad \textbf{(6)}$$

Where $\boldsymbol{C_0}$ (µg/L) is the initial concentration, $\mathbf{C_r}$ (µg/L) is the residual concentration, **m** (g) is the mass of the adsorbent, and **V** (mL) is the solution volume.

At equilibrium, the residual concentration is designated as $\mathbf{C_e}$ (µg/L) and the amount adsorbed as $\mathbf{Q_e}$(µg/g).

The primary models utilized in this study for the description of liquid-solid adsorption isotherms and the conduction of kinetic analyses are presented in **Table I** [10]

Table I: Equations (7) and (8) of the adsorption isotherm and equations (9) and (10) of the kinetic models

Isotherm		**Kinetics**	
Langmuir		Pseudo-First Order	
$\boldsymbol{\frac{C_e}{Q_e} = \frac{1}{K_L Q_{max}} + \frac{C_e}{Q_{max}}}$	**(7)**	$\boldsymbol{\ln(Q_e - Q_t) = \ln Q_e - k_1 t}$	**(9)**
Freundlich		Pseudo-Second Order	
$\boldsymbol{\ln Q_e = \ln K_F + \frac{1}{n} \ln C_e}$	**(8)**	$\boldsymbol{\frac{t}{Q_t} = \frac{1}{k_2 Q_e^2} + \frac{t}{Q_e}}$	**(10)**

Where $\mathbf{Q_t}$ (µg/g) is the amount adsorbed at time **t** (min), $\mathbf{Q_{max}}$ (µg/g) is the maximum adsorption capacity, $\mathbf{K_L}$ (L/µg) is the Langmuir constant, $\mathbf{K_F}$ ((µg/g)(L/µg)$^{1/n}$) is the Freundlich constant, **n** (dimensionless) is the heterogeneity factor reflecting the distribution of adsorption energies, $\mathbf{k_1}$(min^{-1}) is the pseudo-first-order rate constant, $\mathbf{k_2}$ ($g.\mu g^{-1} min^{-1}$)is the pseudo-second-order rate constant, and **t** (min) represents time.

3. Results

3.1. Characterization of raw materials

3.1.1. Physico-chemical characteristics

A pragmatic approach to the analysis of particle size distribution was realised through the graphical representation of the percentages of sand, silt, and clay on the textural triangle (**Figure 3**). This method was utilised to ascertain the soil textural class.

The particle size analysis (**Table II**) showed that clay was the dominant fraction (60.0%). In accordance with the USDA/FAO textural classification [18], the TKA sample was therefore classified as a clay soil.

The physicochemical properties of the clay under scrutiny are presented in **Table III**. The elevated pH (greater than 7.0) indicates the presence of 2:1-type clay minerals, including illite, smectite and vermiculite [30]. The point of zero charge ($\mathbf{pH_{PZC}}$) of the material is 6.62. Below this pH, the surface is positively charged, whereas above it, the surface is negatively charged, favoring the adsorption of anionic and cationic species, respectively [31]. Consequently, it is hypothesized that the adsorption of lead ions from an aqueous solution will be favored at pH values greater than 6.62. The measurement of clay electrical conductivity is a valuable tool that provides insight into the concentration of exchangeable base cations within the interlayer spaces. This, in turn, allows for the assessment of the salinity status of the material. In accordance with the classification scale proposed by Durand J.H. (1983), the electrical conductivity (CE) value of 85.00 µS/cm falls within the range of 0-500 µS/cm. This finding indicates that the studied clay material, TKA, is non-saline [32]. The measured moisture content (H) is 3.18%, indicating a low water retention capacity and suggesting that the TKA sample is essentially non-hygroscopic. The relative density of such minerals is influenced by their mineralogical composition, water content, and degree of compaction. The relative density (d) is approximately 2.27, a value that falls within the typical range reported for typical clay soils. The swelling index (SI) of the TKA sample was measured at 2.71 cm³ per 2 g of clay material. This value falls within the range of 2.50-3.00 cm³/2, indicating that the studied clay belongs to the category of soils susceptible to significant volumetric variations **[33]**. Hebert et al., (2015) [38] demonstrated that the swelling index increases with higher smectite content, while kaolinite and illite/mica also exert a measurable influence. It is well established that the presence of expansive clay minerals, particularly vermiculite, is strongly correlated with high swelling potential in clays. The colloidality of the TKA sample (C) is 7.10%, which is a relatively low value. This can be attributed to the limited ionization of the constituent particles [34]. This characteristic is indicative of the material exhibiting poor dispersion in an aqueous medium. In the context of the extraction of heavy metals from aqueous solutions, higher colloidality is generally considered favourable, as it has been demonstrated to enhance the adsorption of metal ions onto the material surface. The loss on ignition (LOI) of the clay sample is 12.13%, which is indicative of a coexistence of clay minerals with associated minerals [10].

As illustrated in **Table IV**, the organic matter (OM) content of the TKA sample has been determined to be 4.97%. As posited by the classification proposed in the UNDP/FAO project Gui 72/004, this value indicates that the studied clay is rich in organic matter [35]. A high organic matter content can enhance metal adsorption through the formation of stable complexes. Gossart P. (2001) [36] demonstrated that specific functional groups, such as carboxyl, phenol, and amine groups, are capable of forming stable complexes with lead (Pb), cadmium (Cd), and zinc (Zn). Consequently, the organic matter content may be regarded as a pivotal factor when selecting a clay for the immobilization of certain metal cations in aqueous environments.

Table II: Proportion of clay, silt and sand (%) in TKA

Interpretation	Clay	Silt	Sand
TKA	60.00	33.00	7.00

Table IV: Organic carbon (OC) and organic matter (OM) in the TKA sample

OC (%)	OM (%)
2.88	4.97

Table III: Physico-chemical parameters of TKA sample

pH	pH_{pzc}	CE (µS/cm)	H (%)	d	SI (cm^3/2g)	C (%)	LOI (%)
7.61	6.62	85.00	3.18	2.27	2.71	7.10	12.13

Table V: Exchangeable cations (%) and CEC at pH 7 (meq/100 g of clay)

Calcium	Magnesium	Potassium	Sodium	Som of the bases	CEC pH7
14.80	12.40	0.12	0.19	28.00	46.00

Table VI: Surface and porous structure parameters of clay material

S_{BET} (m^2/g)	S_{micro} (m^2/g)	S_{ext} (m^2/g)	V_{micro} (cm^3/g)	V_P (cm^3/g)	D_P (nm)
86.82	12.87	73.95	$6.04.10^{-4}$	0.19	3.24

S_{BET}: BET specific surface area; **S_{micro}:** micropore area; **S_{ext}:** External surface area; **V_{micro}**: Micropore volume; **V_P**: pore volume; **D_P**: pore diameter

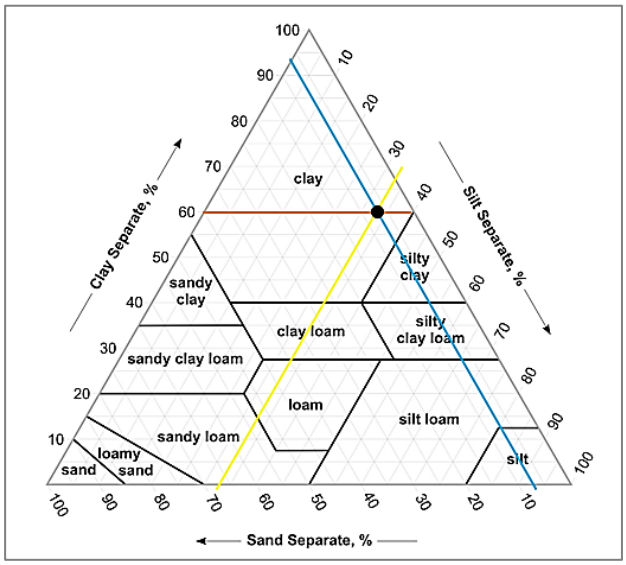

Figure 3: Soil textural triangle

As demonstrated by the findings outlined in **Table V**, calcium and magnesium are the primary exchangeable cations. Chouchane et al. (2011) demonstrated that the sorption of lead by sawdust in an aqueous environment predominantly occurs via a cation-exchange mechanism, wherein exchangeable base cations assume a pivotal role [37]. Nevertheless, elevated concentrations of divalent exchangeable cations such as Ca^{2+} and Mg^{2+} on clay surfaces may inhibit the adsorption of heavy metals, including Pb^{2+}, Cd^{2+}, and Zn^{2+} [38]**.** The cation exchange capacity (CEC) of the clay under scrutiny is marginally elevated in comparison to the values documented for pure illite (20 to 40 meq/100 g) [30, 39]**.** This finding indicates that the material may comprise illite in conjunction with other clay minerals, thereby enabling its categorisation within the group of clay materials that demonstrate a moderate capacity for metal adsorption [40].

3.1.2. Chemical and mineralogical characteristics

The results of the IR analysis are presented in **Figure 4** and **Table VII**. These results highlight the principal functional groups of aluminosilicates, as well as other chemical functionalities. These functionalities govern the clay's interaction with pollutants.

Bands observed between 3200 and 3800 cm^{-1} are assigned to the stretching vibrations of internal O–H groups, whereas those between 1600 and 1700 cm^{-1} correspond to the bending vibrations of the O–H groups associated with structural water [42, 43]. The intense bands observed between 900 and 1200 cm^{-1} are attributed to the stretching vibrations of the Si–O–Si bond [42, 43]. Bands near 800 cm^{-1} correspond to Si–O bending vibrations, while those around 460 cm^{-1} are associated to Si–O rocking vibrations. The bands observed between 795 and 748 cm^{-1} are ascribed to the Si–O–Al linkage [42, 43]. The absorption bands observed around 520 cm^{-1} and 700 cm^{-1} are attributed to Fe–O bending and Fe–O

Table VI provides a synopsis of the textural characteristics of the investigated clay. The BET specific surface area was found to be 86.82 m^2/g, with an external surface area of 73.95 m^2/g and a micropore surface area of 12.87 m^2/g. The external surface area falls within the range reported for illite (65–100 m^2/g) and is slightly lower than that of pure smectite (≈80 m^2/g) [39]. Moreover, the external surface area of the studied material is comparable to that of a natural clay investigated by Bagane M. (2000), which exhibited a value of approximately 71.00 m^2/g [41]. The total specific surface area of 86.82 m^2/g falls within the typical range reported for smectic clay minerals (40–800 m^2/g) [35]. The measured micropore volume was 6.04×10^{-4} cm^3/g, which corresponds to approximately 0.32% of the total pore volume (0.19 cm^3/g). The pore size distribution, determined using the Barrett-Joyner-Halenda (BJH) method, indicates a predominantly mesoporous structure, with an average pore diameter of 3.24 nm.

The observations suggest that the TKA is composed of a mixture of clay minerals. The integration of cation exchange capacity data with the existing body of knowledge lends support to the hypothesis of the presence of 2:1 type clay mineral in TKA.

stretching vibrations, respectively, thereby confirming the presence of Fe_2O_3 in the samples [10]. A thorough analysis of the obtained spectra reveals the presence of absorption bands that are indicative of phyllosilicate groups.

The X-ray diffraction patterns (**Figure 5**) showed that the raw clay consisted mainly of quartz, with minor amounts of kaolinite, vermiculite, potassium feldspar and goethite. The prevalence of quartz has been demonstrated to diminish the adsorption of Pb^{2+} [44]. Conversely, the presence of other minerals has been shown to enhance the binding of Pb^{2+}, attributable to their augmented surface reactivity and cation exchange capacities [45].

X-ray fluorescence (XRF) analysis was employed to quantitatively determine the major oxides and elemental composition of the investigated material. The corresponding results of TKA are summarized in **Table VIII**. The clay TKA is an iron-rich aluminosilicate, composed mainly of SiO_2 (40.46%), Al_2O_3 (23.84%) and Fe_2O_3 (14.44%). The presence of MgO, K_2O and Na_2O confirms the existence of exchangeable basic cations and vermiculite/feldspar phases. The SiO_2/Al_2O_3 (1.70) and Al_2O_3/SiO_2 (0.59) ratios indicate, respectively, a high free silica content and low moisture permeability, which is consistent with the low measured moisture content [46].

Mineralogical and chemical analyses identified kaolinite (49.3%), goethite (15.8%), quartz (18.1%), vermiculite (1.5%) and K-feldspar (15.4%) (**Table IX**). The relatively large external surface area of the clay sample is attributed to the presence of smectite and goethite, as previously reported [47]. Moreover, the high abundance of goethite is likely to generate reactive surface sites, thereby enhancing surface complexation processes with metal ions such as lead. Vermiculite is a type of clay with a high cation exchange capacity (CEC). The layered structure of the substance is characterized by a negative charge, which has been demonstrated to facilitate the attraction and retention of metallic cations, including lead, through the mechanisms of adsorption and ion exchange [48].

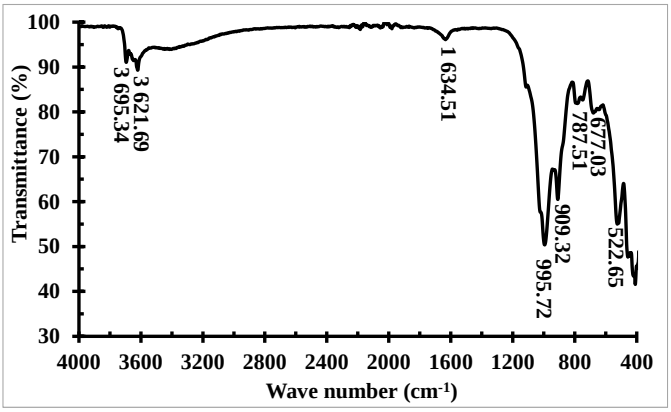

Figure 4: IFTR spectrum TKA sample

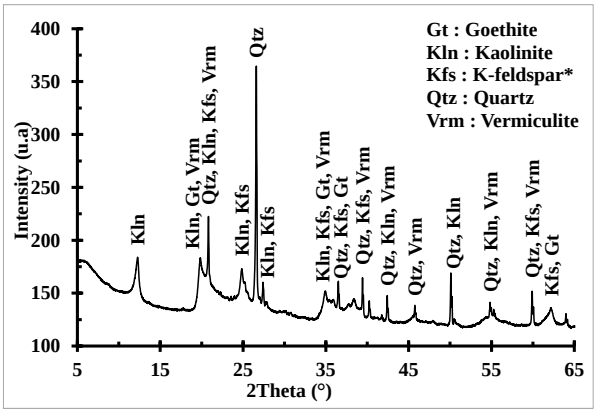

Figure *5*: XRD diffractogram of TKA

Table VII: Main IR bands with their assignments

Bands (cm^{-1})						
3695.34 and 3621.69	1634.51	995.72	909.32	787.51	677.03	522.65
ν_S (O–H)	δ_S(O – H)	ν_S (Si–O)	ν_S (Al–OH)	ν_S (Si–O–Al)	ν_S (Al–OH)	ν_S (Fe–O)

Table VIII: Main oxides

Oxide	**SiO_2**	**Al_2O_3**	**Fe_2O_3**	**CaO**	**MgO**	**K_2O**	**Na_2O**	**P_2O_5**	**TiO_2**
%	40.46	23.84	14.44	<0.01	0.68	0.50	0.14	0.04	2.51

Table IX: Semi-quantitative mineralogical composition of the investigated clay

Mineral phase	**Kaolinite**	**Quartz**	**Goethite**	**Vermiculite**	**K-feldspar**	**Total**
% wt	49.3	18.1	15.8	1.5	15.4	100.00

3.2. Evaluation of the capacity of clay to adsorb lead ions in solution

3.2.1. Optimization of influencing parameters

This study investigates the effects of pH, contact time, adsorbent dosage, and initial lead ion concentration on lead adsorption by TKA, under constant stirring at room temperature.

The adsorption of lead ions was evaluated across a pH range of 3.00 to 7.50, selected to avoid precipitation of Pb^{2+} in solution. The experimental procedure involved the amalgamation of 25 millilitres of a 60 µg/L monometallic Pb^{2+} solution with 0.50 g of clay. The mixture was stirred at a rate of 50 rpm at room temperature, with a contact time of 90 minutes for the clay solution.

pH is a significant parameter in evaluating the adsorption capacity of a clay. In the present study, the pH of the lead solution was modified from 3.00 to 7.50, as demonstrated in Figures 6a and b.

The adsorption experiments conducted at varying pH levels demonstrated a consistent increase in lead removal with rising pH. As demonstrated in Figures 6a and b, the removal efficiency increased from 37.75% at a pH of 3.00 to 69.45% at a pH of 7.50, with the corresponding adsorbed amount rising from 11.30 µg/g to 20.85 µg/g. It is noteworthy that the adsorbed quantities at pH 7.00 and 7.50 were almost equal, suggesting that the optimal pH for lead removal is 7.00 within the experimental parameters employed. The influence of clay mass on Pb^{2+} adsorption was evaluated at pH 7.00 and room temperature, with a contact time of 90 minutes.

Figures 7a and 7b show that the removal efficiency of Pb^{2+} increases with the mass of clay, whilst the adsorption capacity ($\mathbf{Q_{ads}}$) decreases. Although 0.125 g slightly improves removal (81.25% compared to 77.70% at 0.100 g), the latter mass yields a higher $\mathbf{Q_{ads}}$ (11.65 versus 9.75 µg/g), indicating a more efficient use of the adsorbent. Consequently, 0.100 g was selected as the optimal mass, balancing removal performance and adsorption efficiency whilst minimizing material usage and solid waste production.

Utilising the optimised pH and clay mass, Pb^{2+} adsorption exhibited accelerated initial rates and attained equilibrium after 90 minutes, attaining a maximum adsorption capacity of 11.55 µg/g and a removal efficiency of 77.05%. As demonstrated in **Figures 8a** and **8b**, the impact of contact time and initial Pb^{2+} concentration is evident. The determination of equilibrium conditions is instrumental in ascertaining the contact time between Pb^{2+} and the adsorbent.

Pb^{2+} solutions with concentrations ranging from 20 to 120 µg/L were exposed to 0.100 µg of clay for a duration of 90 minutes at ambient temperature. The measurement of residual lead concentrations was undertaken in order to ascertain the initial concentration at which maximum adsorption would be achieved. As shown in **Figures 9a and b**, the adsorption capacity increases with rising initial Pb^{2+} concentration, reaching a maximum at 100 µg/L, beyond which the clay is unable to adsorb additional lead. Conversely, the highest removal efficiency is observed at lower concentrations.

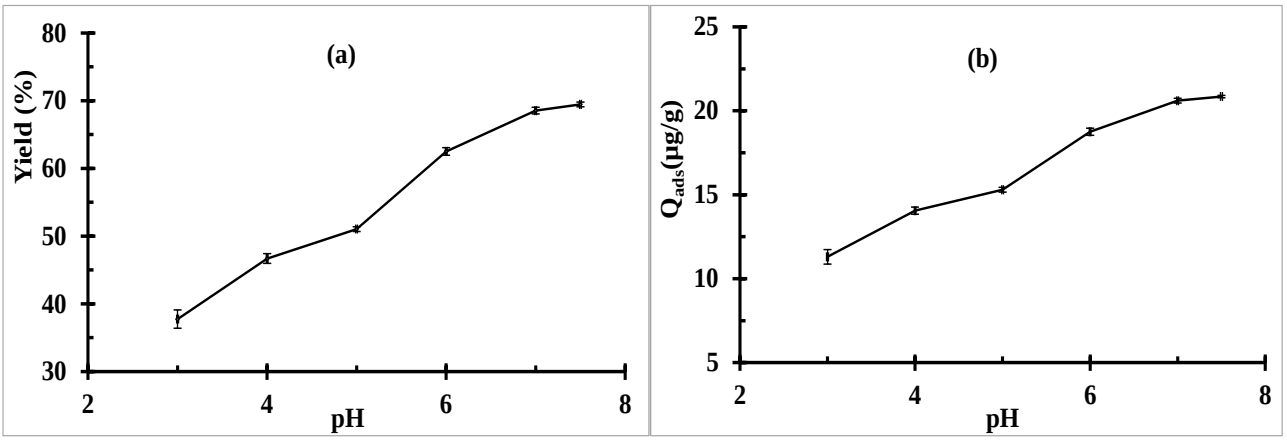

Figure 6: a) pH effect on Pb (II) removal; **b)** Effect of pH on the amount of Pb (II) adsorbed.

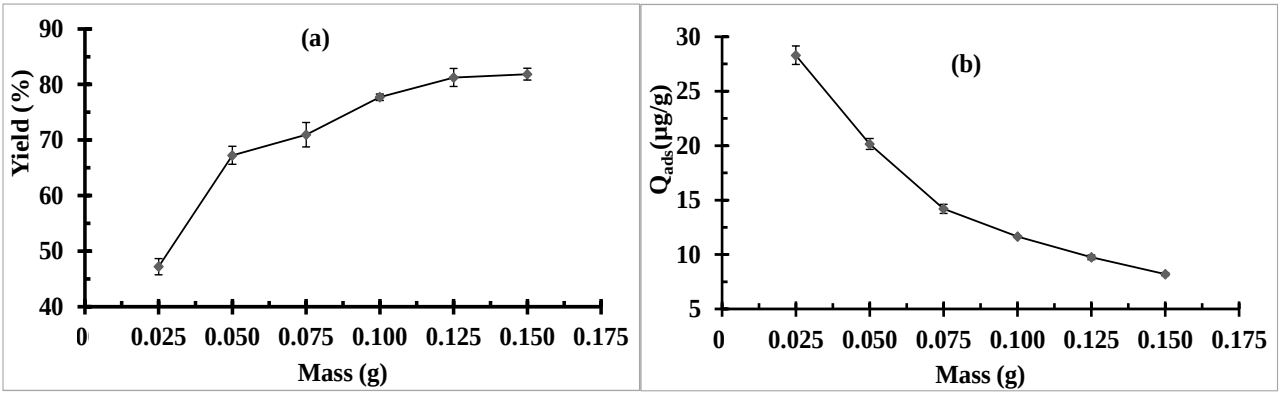

Figure 7: a) Influence of the clay mass on the Pb (II) removal efficiency; **b)** Influence of the clay mass on the amount of adsorbed Pb (II).

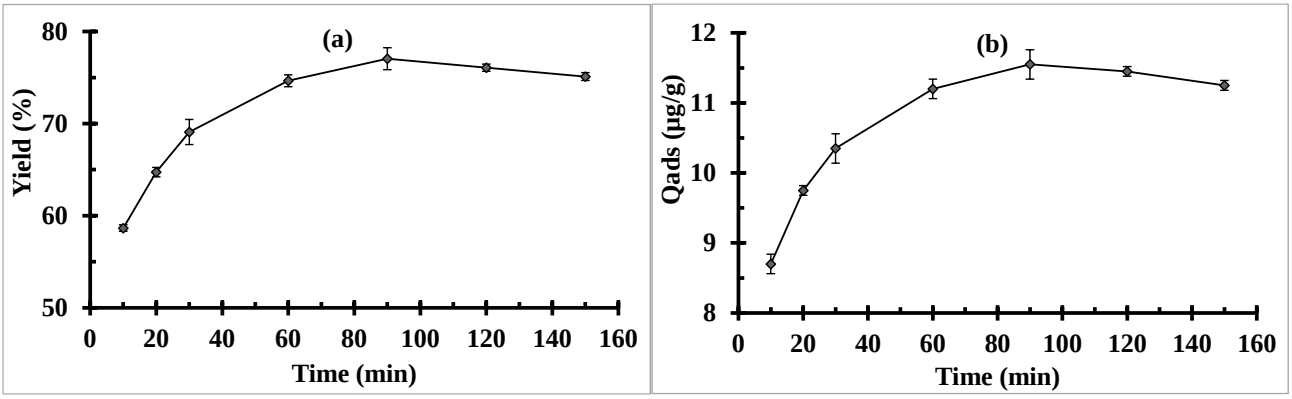

Figure 8: a) Effect of contact time on the yield of Pb (II**); b)** Effect of contact time on Pb (II) adsorption.

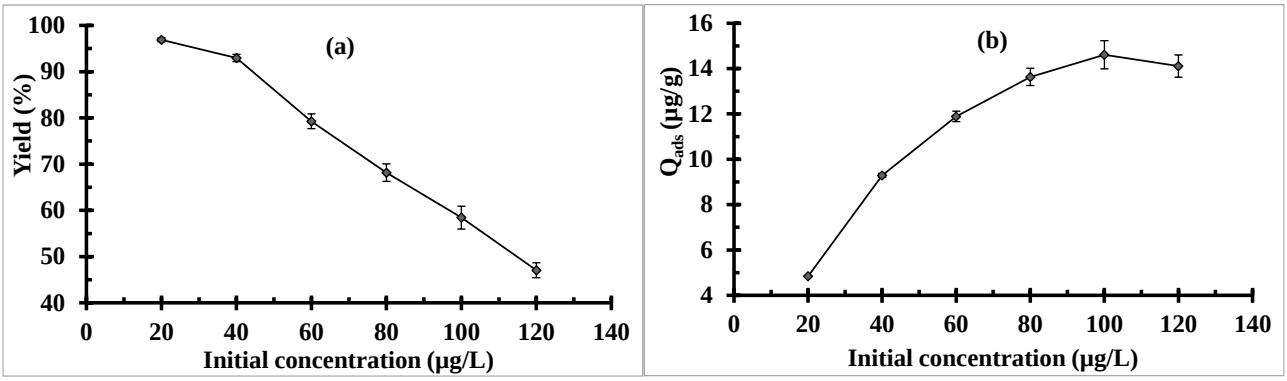

Figure 9: a) Effect of initial Pb^{2+} concentration on removal efficiency; **b)** Effect of initial Pb^{2+} concentration on adsorption capacity.

3.2.2. Adsorption Modeling

The Freundlich and Langmuir adsorption isotherms for the clay are shown in **Figures 10a and b**, with the corresponding parameters in **Table X**. The results indicate favorable adsorption, as evidenced by $0 < K_L < 1$ and $n > 1$, and allow estimation of the theoretical maximum uptake [10]. The Langmuir model proved to be a better fit, as shown by its higher R^2 value, which suggests monolayer adsorption and allows the maximum adsorption capacity to be estimated.

Both the pseudo-first-order and pseudo-second-order kinetic models (**Figures 11a and b**) showed a high degree of linearity ($R^2 > 0.95$). The kinetic parameters are shown in **Table XI.** However, the pseudo-second-order model provided a better fit to the experimental adsorption capacity, suggesting that Pb^{2+} adsorption follows pseudo-second-order kinetics.

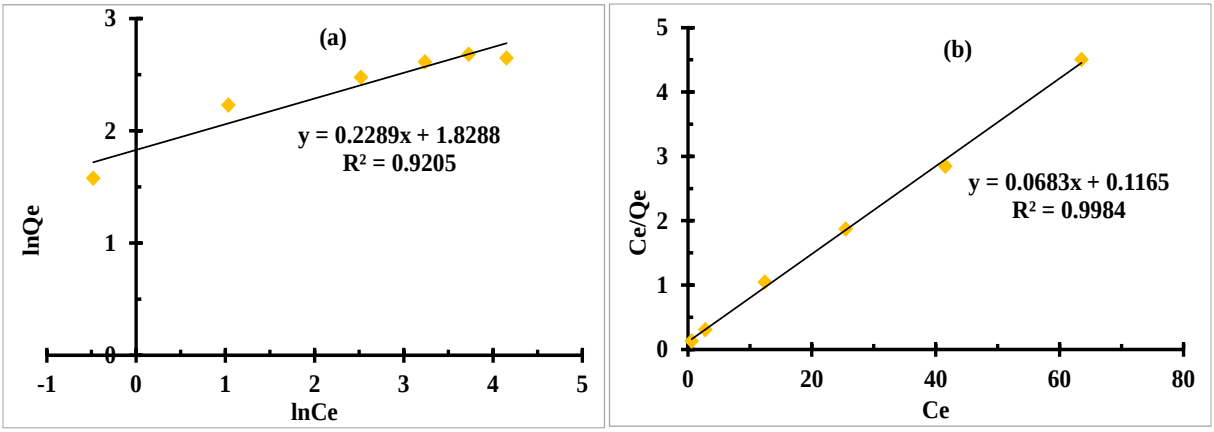

Figure 10 : Plots of **(a)** Freundlich and **(b)** Langmuir

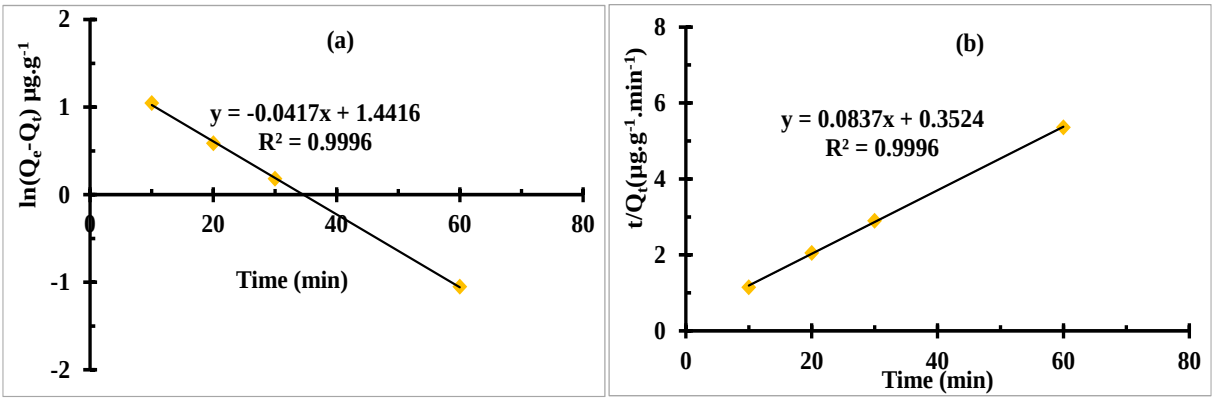

Figure 11: Plots of (a) pseudo-first and (b) pseudo-second-order kinetic for Pb (II) adsorption

Table X: Adsorption conditions, Langmuir and Freundlich constants

Adsorption conditions			**Adsorption constants**					
			Freundlich			**Langmuir**		
T_e (min)	**C_0 (µg/L)**	**m_{ads} (g)**	**K_F ($\mu g^{1-\frac{1}{n}} L^{\frac{1}{n}} g^{-1}$)**	**1/n**	**R**	**K_L(L/µg)**	**Q_{max}(µg/g)**	**R**
90	20-120	0.100	6.23	0.23	0.921	0.57	14.64	0.998

Table XI: Kinetic parameters

Qe_{exp} (µg/g)	**Pseudo-first-order**			**Pseudo-second-order**		
	k_1(min^{-1})	**Qe_{cal}(µg/g)**	**R^2**	**k_2(g.µg^{-1}min^{-1})**	**Qe_{cal}(µg/g)**	**R^2**
11.55	4.17.10^{-2}	4.23	0.9996	1.99.10^{-2}	11.95	0.9996

4. Discussion

The material under study is a clay soil with a slightly alkaline reaction and a lower swelling capacity than sodium bentonite. Conversely, sodium bentonite is a clay with a high alkaline nature and notable dispersive properties, characterized by substantial swelling and a comparatively high Pb(II) adsorption capacity, reported within the range of 10-132 mg.g^{-1} [49]. The pH level of the material (7.6) is comparable to that reported for green clays and distinctly different from that of kaolin. The near-alkaline pH of the solution is conducive to the adsorption of heavy metals, particularly Pb^{2+} ions [50]. he material exhibits a density of 2.27 g/cm³, which is commensurate with that reported for various raw clays examined in Cameroon, South Africa, and Tunisia [51]. The material displays a comparatively elevated swelling potential, with a swelling index ranging between 2.5 and 3 cm³ per 2 g [26]. As indicated by preceding research, heightened swelling indices are typically

correlated with the existence of expandable clay minerals [52]. The colloidal stability of the material in water was assessed through its colloidality, which was found to be 7.1 %. This value is lower than the 9.8% reported by Qlihaa et al. (2015) [53], for a Moroccan clay used as an adsorbent in pollution control and industrial wastewater treatment. The authors attributed this relatively low colloidality to limited ionization of clay particles. The moisture content of the material under study was found to be 3.18%, a factor which could contribute to an increase in the clay's adsorption capacity. Accordingly, the material can be classified as being slightly hydrophilic, a property that is analogous to that of kaolinite [8]. The electrical conductivity is low (85 $\mu S.cm^{-1}$) and markedly lower than that reported for non-saline sodium clays (200-500 $\mu S.cm^{-1}$) [64]. This behavior may be related to a low content of free soluble salts or to the limited release of exchangeable base cations into the aqueous phase **[52]**. The organic matter content is 4.97 %, which is considered moderate according to the literature and is characteristic of natural or slightly weathered surface clays [54]. This value lies near the upper limit of the moderate range, suggesting effective preservation of organic matter within the clay matrix. Such preservation may enhance the cation exchange capacity through the formation of clay-humic complexes [55].

The cation exchange capacity (CEC) of the studied clay (46 meq/100 g) exceeds that typically reported for kaolinite-type clays and is comparable to values observed for charged illite or mixed-layer clays containing smectite [39]. This relatively high cation exchange capacity suggests a composite mineralogy dominated by partially expandable 2:1 phase, such as weakly charged smectites, illite-smectite interstratifications, or the presence of moderate to low proportions of vermiculite. The validity of this interpretation is further substantiated by the chemical composition of the material. The SiO_2/Al_2O_3 ratio (1.70) deviates markedly from that expected for kaolinite (≈1.18) but is consistent with dioctahedral phyllosilicates [56]. In addition, the high Fe_2O_3 content (14.44%) and the presence of MgO (0.68%) indicate the occurrence of isomorphic substitutions ($Fe^{3+} \leftrightarrow Al^{3+}$ and $Mg^{2+} \leftrightarrow Al^{3+}$) within the octahedral sheets. It is well established that such substitutions have the effect of enhancing the permanent structural charge of 2:1 clay layers, and consequently increasing their cation exchange capacity [52]. Furthermore, the negligible presence of calcium oxide (CaO) (< 0.01%) and the minimal levels of sodium oxide (Na_2O) (0.14%) indicate that carbonates and alkali feldspars do not substantially dilute the clay fraction. This lends further support to the mineralogical interpretation based on a predominant 2:1 phyllosilicate structure. The chemical data demonstrate that the clay is predominantly composed of dioctahedral 2:1 layer, exhibiting moderate octahedral substitutions, a finding that is in agreement with the measured CEC. The negligible CaO content indicates an absence of carbonates and the predominance of phyllosilicates, a finding that is consistent with the results of IR and X-ray diffraction (XRD) analyses. These reveal a mixed assemblage of vermiculite, kaolinite, potassium feldspar, goethite and quartz. The clay has a partially expandable structure due to swelling phases and Fe–Mg isomorphic substitution, which gives it a high adsorption potential.

Thus, the combined action of the mineral phases that make up the clay material is responsible for the adsorption of lead ions. However, each mineral's surface properties, charge distribution, and chemical reactivity determine its proportionate contribution. Among these clay minerals, vermiculite emerges as the most efficient phase for Pb^{2+} adsorption, owing to its high specific surface area, substantial interlayer spacing, and pronounced negative surface charge, [52]. Bhattacharyya and Gupta (2008) [57] showed that vermiculite significantly outperforms kaolinite in terms of Pb^{2+} adsorption capacity**.** Vermiculite's strong adsorption is primarily controlled by three mechanisms: dominant cation exchange, surface complexation, and interlayer sequestration [58]. The contribution of potassium feldspar to lead removal is negligible relative to that of vermiculite and kaolinite, which can be attributed to its low specific surface area and weak surface charge [59]. Previous studies have demonstrated that even trace amounts of goethite may significantly enhance lead adsorption, owing to the high reactivity of its surface hydroxyl functional groups [60]. In contrast, quartz is generally regarded as an inert phase, and its role in lead adsorption remains minimal due to its low surface reactivity and the absence of a significant permanent surface charge [61].

The pore size distribution, as determined by the Barrett-Joyner-Halenda (BJH) method, indicates that the sample possesses an average pore diameter ranging from 2 to 50 nm, consistent with mesoporous materials. The measured specific surface area (86.82 m^2/g) is substantially higher than that reported for certain raw clays employed in heavy metal removal from aqueous solutions [62]. This enhancement is attributed to the sample's chemical composition, particularly its elevated Fe_2O_3 content [63]. The external surface area is comparable to that of a natural clay material investigated by Bagane (2000),

which was approximately 71 m²/g [41], and falls within the range reported for goethite (20-80 m²/g) [63].

Adsorption increases sharply with rising pH up to approximately 7, after which a gradual deceleration is observed until pH 7.5. This behavior indicates that an increase in pH renders the clay surface more negatively charged, thereby reducing the interference of H^+ ions with Pb^{2+} ions and favoring lead adsorption [8]. The initial rapid increase can be attributed first to the progressive deprotonation of surface sites, which enhances the negative surface charge and promotes Pb^{2+} uptake, and second, to the stability of Pb^{2+} ions within this pH range [64]. Beyond pH 7, the adsorption capacity declines slightly, likely due to competition with OH^- ions and potential precipitation of Pb^{2+}. Hence, lead adsorption is governed by the clay's surface charge, the competition between H^+ and Pb^{2+} ions, and the speciation of lead [38]. The removal efficiency rises from 47.21% to 81.85% as the adsorbent mass increases from 0.025 g to 0.150 g. Conversely, the adsorption capacity (µg/g) decreases. This behavior can be attributed to the simultaneous effects of an increased number of available active sites with the addition of clay, and the underutilization of sites resulting from an excess of adsorbent [65]. The adsorption kinetics exhibit a rapid uptake during the first 60 minutes, followed by stabilization around 90 minutes. The initial fast adsorption is attributed to the abundance of available active sites on the clay surface, whereas adsorption slows as these sites become increasingly occupied, eventually approaching saturation. Once saturation is reached, a slight desorption is observed, as reflected in the adsorbed quantity. The pseudo-second-order kinetic model provides a good fit for the studied adsorbent–solute system. Similar findings were reported by Zhang and Zhang [66] in their investigation of Pb^{2+} adsorption on a natural clay from China. Moreover, several studies have confirmed that lead ion adsorption on clays generally follows pseudo-second-order kinetics [9, 10]. With increasing initial Pb^{2+} concentration, the removal percentage decreases, whereas the adsorbed amount (Q_e, µg/g) increases. This behavior can be attributed to the enhanced concentration gradient between the solution and the clay surface, which promotes the transfer of lead to the adsorbent [67]. The adsorption isotherm of Pb^{2+} on the studied clay is well described by the Langmuir model, indicating that lead removal occurs predominantly via monolayer adsorption. The adsorption process is strongly influenced by pH, clay dosage, contact time, and initial concentration. At an initial Pb^{2+} concentration of 20 µg/L, optimization of these parameters results in a maximum removal efficiency of 96.90%, underscoring the considerable potential of this clay for water purification, particularly for surface waters, which typically exhibit low lead concentrations with a median value of approximately 5.8 µg/L [68]. The present study demonstrates that static systems are inherently incapable of achieving complete removal of lead at trace concentrations (µg/L), thus emphasising the necessity of dynamic configurations with enhanced mass transfer to ensure consistent and reproducible performance.

5. Conclusion

This investigation of TKA for its application in the adsorption of metal ions produced important outcomes and enabled the characterization and assessment of its capacities. The mineralogical composition of the subject is primarily quartz and kaolinite, with smaller amounts of vermiculite. The predominant oxides identified in this study include iron oxide, silica, and alumina. The material can be categorized as a swelling clay if the swelling index falls between 2.5 and 3 cm³/2 g. The analysis of the effects of solution pH, clay dosage, clay-solute contact period, and starting solute concentration on the adsorption capacity indicates that lead removal from aqueous solutions is possible. The removal effectiveness achieved 96.90% under ideal conditions, which included a clay mass of 0.100 g, a pH of 7; 25 mL of a lead solution at 20 µg/L, and a contact time of 90 minutes. The Langmuir model provides a satisfactory description of the Pb^{2+} adsorption isotherm on the clay under study, with a maximum adsorption capacity of 14.64 µg/g. Furthermore, the pseudo-second-order model is found to be consistent with the adsorption kinetics. These findings suggest that the clay is a natural lead adsorbent that might be used to clean lead-contaminated water.

CRediT authorship contribution statement

Constant ALLARAMADJI NGARMADJI: Writing – review & editing, Writing – original draft, Resources, Methodology, Conceptualization. Kassoum BARRY and Joël SAMBA: Writing – review & editing, Writing– original draft, Resources. Youssouf SAWADOGO: Writing – review & editing, Writing – original draft, Validation, Supervision. Moustapha SAWADOGO: Writing – review & editing, Visualization. Mohamed SEYNOU: Writing – review & editing, Validation, Supervision. Lamine ZERBO: Writing – review & editing, Validation, Supervision.

Funding

This research did not receive any specific grant from funding agencies in the public, commercial, or not-for-profit sectors.

Declaration of competing interest

The authors declare that they have no known competing financial interests or personal relationships that could have appeared to influence the work reported in this paper.

6. References

[1] Abeer A A. Clay basics and their physical and chemical properties: Review Paper. IAETSD J. Adv. Res. Appl. Sci., 2022;10(8):13–18.

[2] Zagalo A H, Noubaimi A A, Szymkiewicz S B, Burlon S, Wouatong A S L. Caractérisation géotechnique des matériaux argileux du 10ème arrondissement de la ville de N'Djamena (Tchad) en vue de leur utilisation comme briques cuites. Sci. Appliquées L'Ingénieur. 2021;3(1):1–7.

[3] Zagalo A H, Rochette P, Wilfried T G. Valorization of Clay Soils from Traditional Quarries in the City of ATI (CHAD) for use as Fired Bricks. Int. J. Curr. Res. Acad. Rev., 2022;10(7):42–51. https://doi.org/10.20546/ijcrar.2022.1007.002.

[4] Oumar A A, Soultan M, Ali A, Jonas T, Saleh A. Physico-chemical and mechanical characterization of local building materials in chad. Int. J. Adv. Res., 2023;11(03):744–754. https://doi.org/10.21474/IJAR01/16490.

[5] Ali A, Mahamat A D, Ban-Nah A, Donnot A, Soultan M. Measurement of the Thermal Conductivities of Clay Materials Stabilized by a Mixed Binder. Phys. Sci. Int. J., 2023;27(3)1–8. https://doi.org/10.9734/psij/2023/v27i3790.

[6] Maoudombaye T, Nodjiasmbayel D, Ngakou A. Analyse en Composantes Principales des Paramètres Physicochimiques et Bactériologiques des Ressources en eaux Destinées à la Consommation dans le Bassin Pétrolier de Doba au Tchad. Eur. Sci. J. ESJ, 2023;24: 660–676. https://doi.org/10.19044/esipreprint.12.2023.p660.

[7] Digué T M, Tinda D, Bertrand N G, Salomon M B, Dikdim D J.-M, Mianpereum T. Contamination and Potential Risks of Heavy Metals in the Sediments of the Chari and Logon Rivers in N'Djamena, Chad. Open J. Soil Sci., 2023;13(02):29–45. https://doi.org/10.4236/ojss.2023.132002.

[8] Maazou A M, Adamou R, Konaté M, Alassane A, Adel M. Valorisation de deux matériaux argileux de la vallée du fleuve Niger dans l'élimination du cuivre des eaux de consommation. J. Soc. Ouest-Afr. Chim., 2017;043 :64 – 75

[9] Hadj B, Messaoud C. Etude de la Fixation des Micropolluants Métalliques (Pb^{2+}, Cd^{2+}) sur une Argile Locale. J. Soc. Ouest-Afr. Chim. 2008;025:63 – 70

[10] Sawadogo L, Barry K, Tchakala I, Sawadogo M, Ouedraogo M, Sory N, Sawadogo Y, Zerbo L, Paré S, Seynou M. Eco-friendly Treatment of Industrial Wastewater with Local Raw Clay. ACS EST Water, 2025; 5(6):3216–3229. https://doi.org/10.1021/acsestwater.5c00089.

[11] Organisation Mondiale de Santé. Directives sur la qualité de l'eau de boisson: Quatrième édition intégrant le premier additif, Genève. 2017.

[12] Union Européenne. DIRECTIVE (UE) 2020/2184 DU PARLEMENT EUROPÉEN ET DU CONSEIL du 16 décembre 2020 relative à la qualité des eaux destinées à la consommation humaine, Strasbourg.

[13] Chowdhury I R, Chowdhury S, Mazumder M A J, Al-Ahmed A. Removal of lead ions (Pb^{2+}) from water and wastewater: a review on the low-cost adsorbents. Appl. Water Sci., 2022;12(8):185. https://doi.org/10.1007/s13201-022-01703-6.

[14] FAO. Synthèse des études thématiques sur la foresterie urbaine et périurbaine de N'Djamena: Appui à la formulation d'une stratégie et d'un plan d'action urbaine et périurbaine à N'Djamena, République du Tchad. Rome, Document de travail sur la foresterie urbaine et périurbaine. 2012;n°7.

[15] Pansu M, Gautheyrou J, Loyer J Y. L'analyse du sol: échantillonnage, instrumentation et contrôle. Paris Milan Barcelone: Masson. 1997.

[16] Callender E. Heavy Metals in the Environment-Historical Trends. in Treatise on Geochemistry, Elsevier, 2003; 67–105. https://doi.org/10.1016/B0-08-043751-6/09161-1.

[17] Buol S W, Southard R J, Graham R C, McDaniel P A. Soil Genesis and Classification. 1re éd. Wiley, 2011. https://doi.org/10.1002/9780470960622.

[18] Mbonigaba J M, Nzeyimana I, Bucagu C, Culot M. Caractérisation physique, chimique et microbiologique de trois sols acides tropicaux du Rwanda sous jachères naturelles et contraintes à leur productivité. Biotechnol. Agron. Soc. Environ., 2009;13:545–555.

[19] Sawadogo Y, Zerbo L, Sawadogo M, Seynou M, Gomina M, Blanchart P. Characterization and use of raw materials from Burkina Faso in porcelain formulations. Results Mater., 2020;6:100085. https://doi.org/10.1016/j.rinma.2020.100085.

[20] D18 Committee Test Methods for Specific Gravity of Soil Solids by Water Pycnometer. 2023. https://doi.org/10.1520/D0854-23.

[21] AFNOR NF EN ISO 10390: Sols, biodéchets traités et boues - Détermination du pH. 2022.

[22] ISO 11265: Environmental solid matrices Determination of the specific electrical conductivity. 2025.

[23] Tchakala I, Bawa L, Djaneye-Boundjou G, Doni K, Nambo P. Optimisation du procédé de préparation des Charbons Actifs par voie chimique (H_3PO_4) à

partir des tourteaux de Karité et des tourteaux de Coton. Int. J. Biol. Chem. Sci., 2012;6(1):461–478. https://doi.org/10.4314/ijbcs.v6i1.42.

[24]NF P84-703. Géosynthétiques bentonitiques – Détermination de la capacité de gonflement de l'argile dans les géosynthétiques bentonitiques. 2020.

[25]Gillott J E. Clay in engineering geology. in Developments in geotechnical engineering, no. 41. Amsterdam: Elsevier. 2012.

[26]AFNOR, NF X31-130. Qualité des sols - Méthodes chimiques - Détermination de la capacité d'échange cationique (CEC) et des cations extractibles. 1999.

[27]ASTM C1069-09. Standard Test Method for Specific Surface Area of Alumina or Quartz by Nitrogen Adsorption. 2022.

[28]Pauwels S J, Ranst E, Verlo M, Mvondo A. Manuel de laboratoire de géologie, méthodes d'analyses des sols et des plantes, équipements, gestion des stocks et des produits chimiques », Publ. Agric., 1992;26:265.

[29]Yvon J, Liétard O, Cases J-M, Delon J-F. Minéralogie des argiles kaoliniques des Charentes. Bull. Minéralogie, 1982;105(5):431–437. https://doi.org/10.3406/bulmi.1982.7565.

[30]Kumari N, Mohan C. Basics of Clay Minerals and Their Characteristic Properties. in Clay and Clay Minerals, G. Morari Do Nascimento, Éd., IntechOpen. 2021. https://doi.org/10.5772/intechopen.97672.

[31]Bergaoui L, Lambert J, Suquet H, Che M. Étude des propriétés adsorbantes d'une argile pontée vis-à-vis de Cu^{2+} et Cd^{2+} en fonction du pH », J. Chim. Phys., 1995;92:1486–1505. https://doi.org/10.1051/jcp/1995921486.

[32]Durand J H. Les sols irrigables: étude pédologique. in Techniques vivantes. Paris: Agence de coopération culturelle et technique: Presses universitaires de France. 1983.

[33]Hubert H, Nicolas M, Delphine B, Adrien L C. Test de la mesure de l'indice de gonflement des sols par immersion dans l'eau pour la caractérisation du retrait-gonflement de sols naturels. Présenté à International Symposium Shrink-swell processes in soils - Climate and constructions, Marne-La-Vallée, France, 2015;p. 11.

[34]Rollet A P. L'analyse thermique. Gauthier-Villars. 1972.

[35]Panagos P, Jones A, Bosco C, Kumar P S S. European digital archive on soil maps (EuDASM): preserving important soil data for public free access. Int. J. Digit. Earth, 2011;4(5):434–443. https://doi.org/10.1080/17538947.2011.596580.

[36]Gossart P. Contribution à l'étude des interactions de la matière organique des sols avec les métaux lourds : étude structurale et analytique de molécules modèles. PhD, Lille, France. 2001.

[37]Chouchane T, Chouchane S, Boukari A, Balaska A, Samar M H. Elimination du plomb en solution par la sciure de bois. Rev. Energ. Renouvelables. 2011;14(4):613–626.

[38]Serpaud B, Al-Shukry R, Casteignau M, Matejka G. Adsorption des métaux lourds (Cu, Zn, Cd et Pb) par les sédiments superficiels d'un cours d'eau: rôle du pH, de la température et de la composition du sédiment. Rev. Sci. Eau. 2005;7(4):343–365. https://doi.org/10.7202/705205ar.

[39]Morel R. Les sols cultivés. Paris: Lavoisier. 1996.

[40]Thomas T. L'adsorption des produits pharmaceutiques par interactions organo-minérales: processus et applications environnementales », PhD, Orléans, France. 2015.

[41]Bagane M. Elimination d'un colorant des effluents de l'industrie textile par adsorption », Ann. Chim. Sci. Matériaux. 2000;25(8):615–625. https://doi.org/10.1016/S0151-9107(00)90003-5.

[42]Diadi T, Sawadogo Y, Sorgho B, Sawadogo M, Seynou M, Zerbo L, Blanchart P. Valorization of Glass Bottles in the Manufacture of Fired Compressed Earth Bricks (CEB). J. Miner. Mater. Charact. Eng. 2025;13(02):44–62. https://doi.org/10.4236/jmmce.2025.132004.

[43] Sory N, Sanou I, Barry K, Sawadogo Y, Ouedraogo M, Zerbo L, Seynou M. Comportement hygrométrique et hydrique des blocs de terre comprimée stabilisés à la poudre de coques d'arachide. J. Soc. Ouest-Afr. Chim. 2025; 054: 85 – 98.

[44]Uddin M K. A review on the adsorption of heavy metals by clay minerals, with special focus on the past decade. Chem. Eng. J. 2017;308:438-462. https://doi.org/10.1016/j.cej.2016.09.029.

[45]Otunola B O, Ololade O O. A review on the application of clay minerals as heavy metal adsorbents for remediation purposes. Environ. Technol. Innov. 2020;18:100692. https://doi.org/10.1016/j.eti.2020.100692.

[46] Jarraya I, Fourmentin S, Benzina M. Adsorption de COV par un matériau argileux tunisien organo-modifié. J. Société Chim. Tunis., 2010;12:139–149.

[47]Sei J, Jumas J C, Olivier-Fourcade J, Quiquampoix H, Staunton S. Role of Iron Oxides in the Phosphate Adsorption Properties of Kaolinites From the Ivory Coast. Clays Clay Miner.

2002;50(2):217–222.
https://doi.org/10.1346/000986002760832810.
[48]Malandrino M, Abollino O, Giacomino A, Aceto M, Mentasti E. Adsorption of heavy metals on vermiculite: Influence of pH and organic ligands. J. Colloid Interface Sci. 2006;299(2):537–546. https://doi.org/10.1016/j.jcis.2006.03.011.
[49]Majiya H, Clegg F, Sammon C. Bentonite-Chitosan composites or beads for lead (Pb) adsorption: Design, preparation, and characterisation. Appl. Clay Sci. 2023;246:107180. https://doi.org/10.1016/j.clay.2023.107180.
[50]Raji Z, Karim A, Karam A, Khalloufi S. Adsorption of Heavy Metals: Mechanisms, Kinetics, and Applications of Various Adsorbents in Wastewater Remediation—A Review. Waste. 2023;1(3):775–805.
https://doi.org/10.3390/waste1030046.
[51]Majouri N, El Mankibi M, Sghaier J. Unlocking The Potential of Tunisian Clays: Sustainable Materials for Energy-Efficient Construction. ACS Omega. 2025;10(27):28874–28886. https://doi.org/10.1021/acsomega.5c00065.
[52]Bergaya F, Theng B K G, Lagaly G. Handbook of Clay Science. Elsevier.
[53]A. Qlihaa, D. Souad, F. Melrhaka, et N. Hajjaji, 2016. Caractérisation physico-chimique d'une argile Marocaine. J. Mater. Environ. Sci. 2006;7(5):1741–1750.
[54]Prout J M, Shepherd K D, McGrath S P, Kirk G J D, Hassall K L, Haefele S M. Changes in organic carbon to clay ratios in different soils and land uses in England and Wales over time. Sci. Rep. 2022;12(1):5162. https://doi.org/10.1038/s41598-022-09101-3.
[55]Nikishina M, Perelomov L, Atroshchenko Y, Ivanova E, Mukhtorov L, Tolstoy P. Sorption of Fulvic Acids and Their Compounds with Heavy Metal Ions on Clay Minerals. Soil Syst. 2022;6(1):2. https://doi.org/10.3390/soilsystems6010002.
[56]Ouattara S, Sawadogo Y, Sawadogo M, Sorgho B, Seynou M, Blanchart P, Zerbo L. Effect of rice husk ash on physical, mechanical, and hydric properties of clay-based geopolymer. Results in Materials. 2025;28 (2025) 100821. https://doi.org/10.1016/j.rinma.2025.100821
[57]Bhattacharyya K G, Gupta S S. Adsorption of a few heavy metals on natural and modified kaolinite and montmorillonite: A review. Adv. Colloid Interface Sci. 2008;140(2):114–131. https://doi.org/10.1016/j.cis.2007.12.008.
[58]Dubus J, Leonhardt N, Latrille C. Multi-cation exchanges involved in cesium and potassium sorption mechanisms on vermiculite and micaceous structures. Environ. Sci. Pollut. Res. 2023;30(1):1579–1594.
https://doi.org/10.1007/s11356-022-22321-4.
[59]Stumm W, Sigg L, Sulzberger B. Chemistry of the solid-water interface: processes at the mineral-water and particle-water interface in natural systems. New York: Wiley. 1992.
[60] Wang X, Cui L, Xiao J, Ding Z. Stable carbon isotope of black carbon in lake sediments as an indicator of terrestrial environmental changes: An evaluation on paleorecord from Daihai Lake, Inner Mongolia, China. Chem. Geol. 2013;347:123–134. https://doi.org/10.1016/j.chemgeo.2013.03.009.
[61]Kosmulski M. Éd., Surface charging and points of zero charge. in Surfactant science series, no. 145. Boca Raton: CRC Press. 2009.
[62]Kouadio L M, Lebouachera S E I, Blanc S, Sei J, Miqueu C, Pannier F, Martinez H. Characterization of Clay Materials from Ivory Coast for Their Use as Adsorbents for Wastewater Treatment. J. Miner. Mater. Charact. Eng. 2022;10(04):319–337.
https://doi.org/10.4236/jmmce.2022.104023.
[63]Cornell R M, Schwertmann U. The iron oxides: structure, properties, reactions, occurrences, and uses. 2nd, completely rev. and extended ed éd. Weinheim: Wiley-VCH GmbH & Co. KGaA. 2003. https://doi.org/10.1002/3527602097.
[64]Hem J D. Geochemical controls on lead concentrations in stream water and sediments. Geochim. Cosmochim. Acta. 1976; 40(6):599–609.
[65]Foo K Y, Hameed B H. Insights into the modeling of adsorption isotherm systems. Chem. Eng. J. 2010;156(1):2–10. https://doi.org/10.1016/j.cej.2009.09.013.
[66]Zhang J, Zhang L. Adsorption behaviors of heavy metal Pb(II) on clay. Chin. J. Geotech. Eng. 2012;34(9):1584–1589.
[67]Jawad A H, Al-Heetimi D T A, Mastuli M S. Biochar from Orange (citrus sinensis) Peels by Acid Activation for Methylene Blue Adsorption. Iran J Chem Chem Eng. 2019;38(2):91–105.
[68] Wei S, Berti E, Ma D, Wu Q, Peng Y, Yuan C, Zhao Z, Jin X, Ni X, Wu F, Yue K. Global patterns and drivers of lead concentration in inland waters. J. Hazard. Mater. 2023;460:132455. https://doi.org/10.1016/j.jhazmat.2023.132455.